Publishing House
AKAPIT

COMPUTER METHODS IN MATERIALS SCIENCE

Informatyka w Technologii Materiałów

Vol. 11, 2011, No. 1

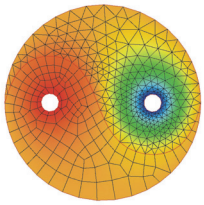

COMPUTER MODELING OF PNEUMATIC FORMATION OF SUPERTHIN FIBRES

LESZEK JARECKI*, SLAWOMIR BLONSKI, ANDRZEJ ZACHARA, ANNA BLIM

Institute of Fundamental Technological Research, Polish Academy of Sciences,
Pawinskiego 5B, 02-106 Warsaw, Poland
**Corresponding author: ljarecki@ippt.gov.pl*

Abstract

Dynamics of a novel pneumatic process of superthin fibres formation from polymer melts in supersonic air jets in the Laval nozzle is studied using computer simulation. The approach bases on the mathematical k-ω models of air flow in the nozzle and air drawing of polymer filaments in the coaxial air jet. The aerodynamic fields can be considered as undisturbed by presence of a single row of thin polymer filaments and predetermined air conditions are used in the modeling. The air fields are simulated for several values of the air compressions in the nozzle inlet and two nozzle geometries. Driving force of the Laval nozzle process results from the air drag forces acting onto the filament surface. Mathematical model of stationary melt spinning in single-, thin-filament approximation is applied with the effects of non-linear viscoelasticity of the polymer melt accounted for. The model allows also to discuss non-linear stress-optical relationship reflecting online molecular orientation, as well as online crystallization of the polymer filament if it occurs.

Negative rheological extra-pressure in the air-drawn filament is predicted, as resulting from non-linear viscoelasticity of the polymer melt subjected to high elongation rates. The negative extra-pressure could lead to cavitation and longitudinal burst splitting of each filament into a high number of superthin sub-filaments. A hypothetical mean diameter of the sub-filaments is estimated from an energetic criterion. Example computations of the dynamic profiles of air drawing and discussion concern isotactic polypropylene (iPP) subjected to the Laval nozzle process.

Key words: melt spinning, polymer air drawing, Laval nozzle process, superthin fibres

1. INTRODUCTION

Superthin fibres with the diameter range 0.1-10 μm show high surface-to-volume ratio of the order of several square meters per cubic centimeter of the raw material and are used for high-surface-activity products, such as filtration mats, nonwovens for biological and medical applications, etc. Pneumatic fibre spinning in supersonic air jets in the Laval nozzle is a novel, efficient and energy saving method of formation of nonwovens of superthin fibres and continuous fibres. The method was patented several years ago by Nanoval company for obtaining superthin fibres from synthetic, natural and biodegradable polymers (Gerking, 2002). Mathematical or computer model which would describe dynamics of melt spinning in the Laval nozzle process is still lacking in the literature.

Schematic illustration of air-drawing of an individual polymer stream in the Laval nozzle pneumatic process is shown in figure 1 at the cross-section normal to the longitudinal spinning beam. In the process, cold air is compressed in the inlet of a longitudinal Laval nozzle to accelerate the air to supersonic velocity in the nozzle outlet. The polymer is co-extruded in the symmetry plane of the air jet from o single row of small-diameter orifices. The polymer streams are subjected to high elongation rates under air drag forces and fall down freely onto

 ISSN 1641-8581

a collector forming a nonwoven mat of superthin fibres at the end of the processing axis. Pneumatic melt spinning is a two-phase process where the velocity, temperature, pressure or stress distributions in each phase, the air and the polymer streams, should be considered. The influence of single row of thin polymer streams on the air jet dynamics can be neglected (Krutka et al., 2003) and predetermined air fields at the absence of polymer filaments are used in the modeling.

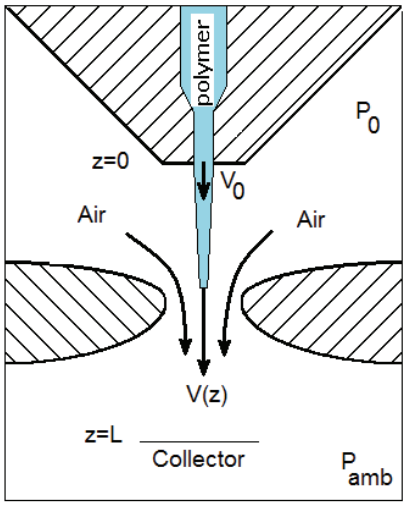

Fig. 1. *Air drawing of a polymer melt in the Laval nozzle process.*

2. AIR FIELDS IN THE LAVAL NOZZLE MELT SPINNING

The air fields important for polymer air drawing are predetermined from the mathematical k-ω model presenting aerodynamic phenomena in the Laval nozzle. Due to high air velocities generating high Reynolds numbers, turbulent flow is considered with the method presented by Wilcox (1988), considering the turbulent kinetic energy $k = < u_i u_i > / 2$ and the specific dissipation rate $\omega = \varepsilon / k$ where the turbulent dissipation rate $\varepsilon = \nu \left\langle \frac{\partial u_i}{\partial x_j} \frac{\partial u_j}{\partial x_i} \right\rangle$ and ν is kinematic viscosity of the air.

Steady-state and compressible air flow is considered in the (y,z) plane of the Carthesian coordinates where x-axis is oriented along the spinning beam with a longitudinal Laval nozzle, and the y-axis is normal to the air jet symmetry plane. The air flow reduces to two-dimensional in the (y,z) plane and axisymmetric for long spinning beams, with the length-to-width ratios above 50 where the end effects can be neglected. The air velocity components U_y, U_z, temperature T, pressure P, density ρ, and the quantities k and ω are computed from the set of mass continuity, momentum, and energy conservation equations, equations of turbulent kinetic energy k, specific dissipation rate of turbulent energy ω, and the ideal gas state equation. The computational domain reduces to the half-plane limited by the $y = 0$ symmetry axis. The computations are performed for two Laval nozzle geometries: with zero-length throat and 8 mm long throat, as presented in figures 2 (a,b).

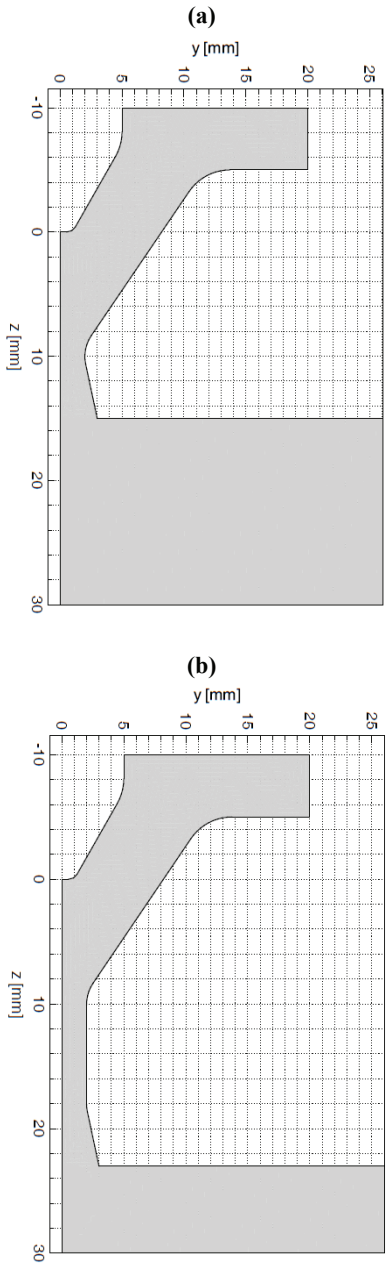

Fig. 2. *Half-plane of the Laval nozzle cross-section limited by the symmetry axis y = 0;(a) zero-length throat, (b) 8 mm long throat. The air flow area is shaded.*

The boundary conditions for the Laval nozzle air fields read:

$$P = P_{amb} + \Delta P_{air}, \quad k = \omega = 0, \quad T = T_{amb} \qquad (1)$$

at the nozzle inlet $z = -10$ mm,

$$P = P_{amb},\ T = T_{amb},\ \frac{\partial k}{\partial z} = \frac{\partial \omega}{\partial z} = 0 \qquad (2)$$

at the domain outlet $y = 100$ mm, $z = 240$ mm,

$$\frac{\partial U_z}{\partial y} = \frac{\partial T}{\partial y} = \frac{\partial P}{\partial y} = \frac{\partial k}{\partial y} = \frac{\partial \omega}{\partial y} = 0,\ U_y = 0 \qquad (3)$$

at the symmetry plane $y = 0$,

$$U_y = U_z = k = \omega = 0, \quad T = T_{amb} \qquad (4)$$

at the walls of the nozzle.

ΔP_{air} is air compression in the inlet, ambient temperature $T_{amb} = 20^{o}$C and pressure $P_{amb} = 1$ bar.

consist of 143 795 grid cells, with the computational error less than 1%. Computations of the air fields were performed for air compressions $\Delta P_{air} = 1$, 2 and 3 bars.

Figures 3 (a,b) illustrate air velocity and temperature fields computed for 2 bars of the air compression and the nozzle with the zero-length throat. Highest air velocities are found at the jet centerline, y=0. Distributions of the Mach number and air temperature along the centerline are presented in figures 4 (a,b) for both nozzle geometries and the initial air compressions. Axial air velocity increases very rapidly, with the Mach number achieving unity inside the nozzle and increasing at the nozzle exit to a maximum of 1.6-1.8. After the maximum, it still

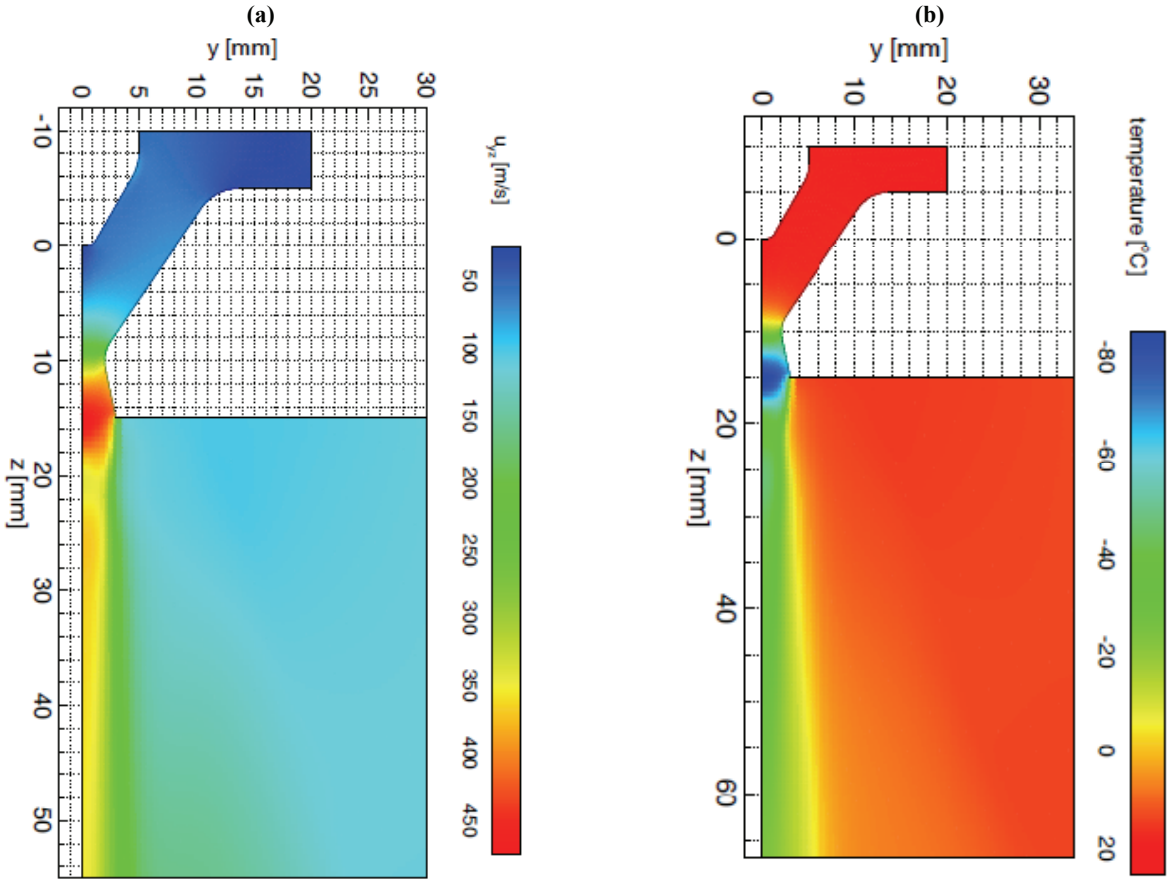

Fig. 3. *Distributions of modular air velocity (a) and temperature (b) in the Laval nozzle and adjacent area computed for $\Delta P_{air} = 2$ bars and zero-length nozzle throat.*

The air fields were computed with the aid of the Fluent package. Several mesh resolution tests were performed to evaluate the grid convergence index GCI (Roache, 1998) and to chose an optimal mesh resolution compromising the computation time and numerical accuracy. The most sensitive region to the mesh resolution is located in the narrowing ranges within the nozzle. Based on the test simulation results in this ranges, an optimal mesh was found to

remains at a supersonic level for $\Delta P_{air} = 2$ and 3 bars. For every inlet compression, the air pressure rapidly drops down to the ambient level and the fast decompression is accompanied by rapid decrease in the air temperature. It remains much below 0°C far after the nozzle exit for the higher inlet compressions. In the case of 8 mm long throat, all the air fields are shifted along the jet axis by a distance of the throat length. One concludes that the highest air

jet potential for fibre spinning locates at the jet symmetry axis with the highest air velocity.

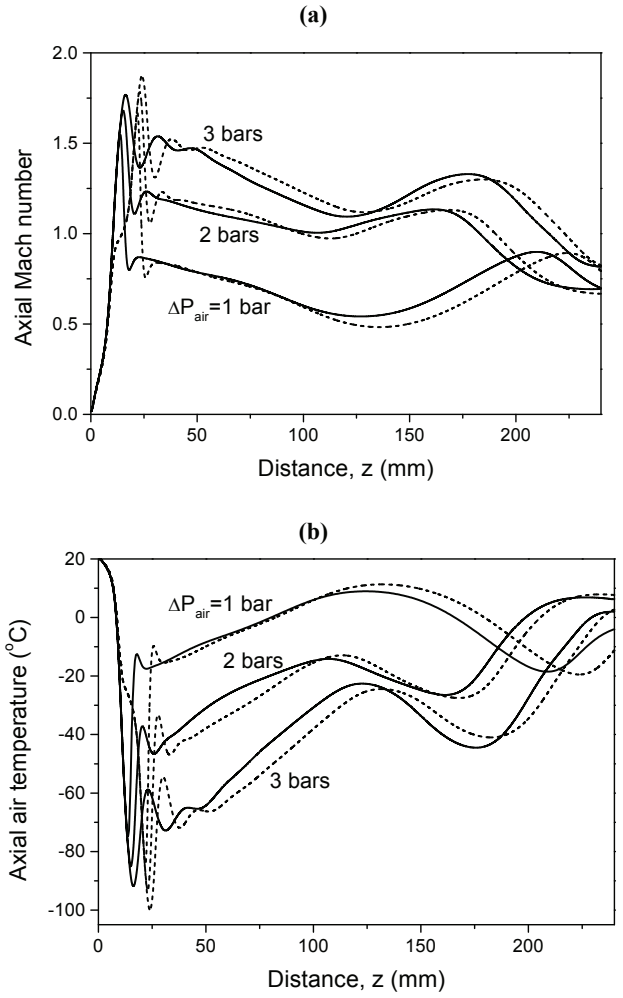

Fig. 4. *Axial profiles of the Mach number (a) and air temperature (b) vs. distance z computed for different ΔP_{air}. Solid lines - zero-length throat, dashed lines – 8 mm long throat.*

3. AIR-DRAWING OF THE POLYMER FILAMENT

In the Laval nozzle process, individual polymer streams are extruded from circular orifices located at the air jet symmetry plane. Computer simulation of air drawing of the polymer filament in the pneumatic process bases on the mathematical model of fibre melt spinning elaborated by Ziabicki et al. (1998) and further modifications of the model for pneumatic processes by Jarecki & Ziabicki (2008). The approach allows to discuss the role of the process and material parameters in the dynamics of air drawing, development of fibre structure and thickness. Fibre air drawing is a uniaxial deformation process with dominating elongational flow of the polymer and negligible contribution of the radial gradient of the axial velocity component. Stationary model of air drawing of polymer melt in single-, thin filament approximation reduces to one dimension z - the axial distance from the polymer extrusion point. Axial polymer velocity $V(z)$, temperature $T(z)$, and the extra-stress components $\sigma_{ij}(z)$ are considered as average values over the radial filament cross-section. Air conditions on the thin filament surface are approximated by the predetermined air fields along the jet centerline.

The stationary air drawing model consists of the mass conservation, force balance and energy conservation equations, constitutive equation of non-linear viscoelasticity and structure development equations considering molecular orientation and crystallinity (Jarecki & Ziabicki, 2008). The equations allow to express axial gradients of five dynamic and structural functions and compute them using the Runge-Kutta integration procedure with stationary initial conditions for the polymer velocity, temperature, tensile stress, extra-pressure, and zero initial crystallinity. The approach is valid in the range of z where local air velocity exceeds local velocity of the filament, $U_z(z) > V(z)$. The air drawing process is driven by air friction shear stress on the filament surface $p_{zr}(z) = -C_f(z)\rho_a(z)[U_z(z) - V(z)]^2$ where $C_f(z) = 0.78 \cdot Re^{-0.61}$ is local air friction coefficient determined from experimental correlations with the Reynolds number Re by Majumdar & Shambaugh (1990), $\rho_a(z)$ – local air density. Contribution of the convective heat exchange between the filament and the air is computed with the heat exchange coefficient determined from the experimental correlations between the Nusselt and Reynolds numbers, $Nu = 0.042Re^{0.334}$ (Bansal & Shambaugh, 1988).

For the deformation rate $\dot{\mathbf{e}}$ and extra-stress σ tensors relationship, Phan-Thien/Tanner constitutive equation of polymer melt non-linear viscoelasticity is used (Larson, 1988)

$$\tau\left[\dot{\boldsymbol{\sigma}} - 2(1-\xi)\boldsymbol{\sigma}\dot{\mathbf{e}}\right] + \boldsymbol{\sigma}\exp\left(\varepsilon\frac{\tau}{\eta}tr\boldsymbol{\sigma}\right) = 2\eta\dot{\mathbf{e}} \qquad (5)$$

where η, τ – zero-shear viscosity and relaxation time, ε, ξ – constants responsible for non-linear and shear-thinning effects, respectively. The computations are performed for iPP with $\varepsilon = 0.015$ and $\xi = 0.6$ used also by Lee et al. (2005). Arrhenius temperature-dependence of the melt viscosity is assumed with the front factor responsible for the effects of entanglements of chain macromolecules. Uniaxial elongational flow deformation of incompressible polymer melt is assumed in the computa-

tions, with elongation rate $\dot{e}$ of the cylindrical filament, local tensile stress $\Delta p(z) = \sigma_{zz}(z) - \sigma_{rr}(z)$ and rheological extra-pressure $p_{rh}(z) = -[\sigma_{zz}(z) + 2\sigma_{rr}(z)]/3$. The model accounts also for the heat of viscous friction generated in the polymer under high elongation rates. For stationary air drawing we have $\dot{e} = dV/dz$ and volume density of the viscous friction heat is given by $\Delta p(z) dV/dz$.

4. RESULTS AND DISCUSSION

Figures 5 (a-f) illustrate axial profiles of polymer velocity, velocity gradient, filament diameter, polymer temperature, tensile stress and the extra-pressure computed for iPP of melt flow rate index MFR = 12 (molecular weight M_W = 250,000), inlet air compressions ΔP_{air} = 1, 2 and 3 bars, and collector located at z = 200 mm. In the nonwovens formation processes, the filaments fall freely onto the collector and the initial filament tension is adjusted by an inverse procedure to zero tension at the free end at the collector. The computations are performed for melt extrusion temperature 300°C, and the initial melt velocity is determined by the orifice diameter of 0.7 mm and the extrusion rate of 0.04 g/sec. Solid-line plots show axial profiles obtained for zero-length Laval nozzle throat, and dashed-line plots – for 8 mm long throat. The filament velocity does not exceed air velocity between the extrusion point and the collector and the air-drawing conditions are satisfied along the entire processing line. Significant impact of ΔP_{air} on the axial filament velocity, elongation rate, filament attenuation, etc. is seen in the figures, but without any particular influence of the throat length.

At ΔP_{air} = 3 bars filament velocity approaches at the collector 50% of the sound velocity, with the maximum of the elongation rate of about 1200 s^{-1} at 1/3 of the processing axis.

The predicted filament velocities are nearly twice higher than those reported for conventional high-speed melt spinning, while the elongation rates are five-six times higher and concentrated within much narrower range of the process axis. Much higher values of the tensile stresses are also predicted for the supersonic process, with the maximum in the middle of the processing line, indicating much higher stream birefringence in the Laval nozzle processes. Majority of the filament attenuation is predicted to take place within a very short distance range of about 50 mm from the extrusion point for each ΔP_{air} value.

The filament temperature drops down by about 100°C between the extrusion point and the collector, but still it is above the polymer crystallization range. Thus, online crystallization of the filament is not predicted, despite air temperature much below 0°C on the processing line. Intensive cooling of the polymer filament in the cold air jet is compensated to a high extent in the computations by the heat of viscous friction in the polymer bulk.

We predict negative rheological extra-pressure p_{rh} created in the filament inside the Laval nozzle throat, at a distance of about 10-20 mm from the extrusion orifice, with the absolute value of the pressure increasing with ΔP_{air}. The extra-pressure results from non-linear viscoelasticity of polypropylene at high elongation rates and may cause cavitation leading to longitudinal burst splitting of the filament into a high number of sub-filaments under the elongational tensile stress. Assuming that energy of the extra-pressure converts in total into the surface energy of sub-filaments during the hypothetical splitting, an average diameter d of the sub-filaments created from a filament of diameter $D(z)$ should read (Jarecki et al., 2011)

$$d \cong -\frac{4\gamma(z)}{p_{rh}(z)} \tag{6}$$

for $-p_{rh}(z) >> 4\gamma(z)/D(z)$ where $\gamma(z) = 2.94\times10^{-2} - 5.6\times10^{-5}\left[T(z) - 296\right]$ is local surface free energy density of iPP (in [N/m]) at absolute temperature T(z). Minimum of the negative extra-pressure is located at a very short distance of 7-10 mm from the extrusion orifice for each air compression value and both nozzle geometries, but with slightly smaller absolute value for 8 mm throat. One concludes that the longer throat does not enhance dynamics of the air drawing process, and it may cause plugging of the nozzle by the polymer at burst splitting predicted inside the nozzle throat.

Figure 6 shows the hypothetic diameter of the sub-filaments vs. ΔP_{air} in comparison with the diameter of the filaments without splitting taken at the collector located 200 mm from the extrusion point. The splitting would reduce the diameter to the range of superthin fibres, between 10 and 4.5 μm for the presented ΔP_{air} values, while the filament diameter without splitting would remain in the range between

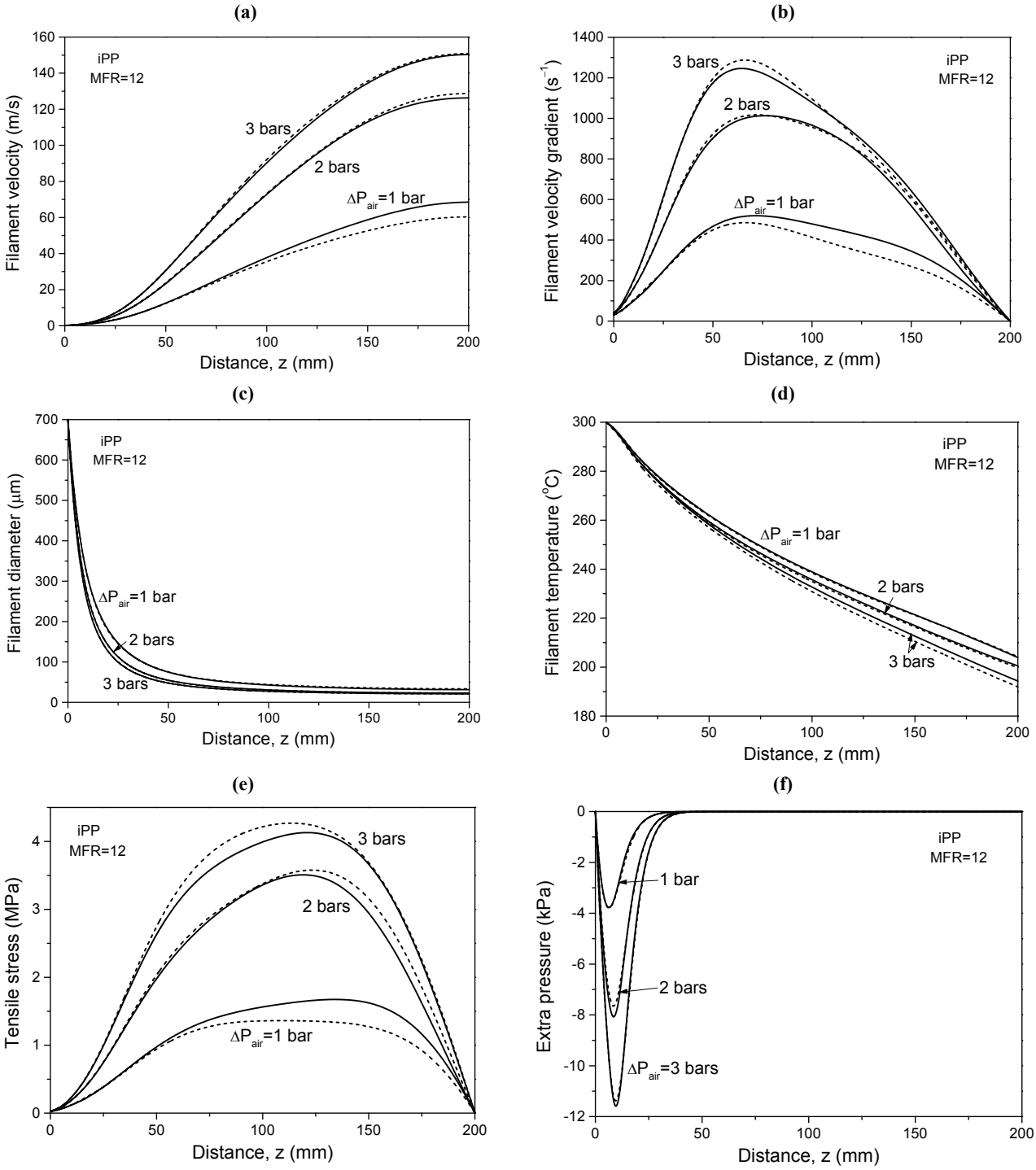

Fig. 5. *Axial profiles of the filament velocity (a), velocity gradient (b), diameter (c) temperature (d), tensile stress (e), and extra-pressure (f) computed vs. distance z for iPP (MFR=12) and several ΔP_{air} values. Melt extrusion temperature - 300°C, orifice diameter - 0.7 mm, extrusion rate - 0.04 g/sec, collector at z=200 mm. Solid lines – zero-length nozzle throat, dashed lines - 8mm throat.*

33 and 21 μm at the collector. The nozzle geometry considered in the computations does not influence the filament diameter. Burst splitting of the filaments in the Laval nozzle process was reported by Gerking (2002) from experimental observations where the average diameter of the sub-filaments remained in the range between 15 and 2 μm.

ACKNOWLEDGEMENT

This paper resulted from the research supported by Research Grant Nr N N507 448437 from the Ministry of Science and Higher Education of the Republic of Poland.

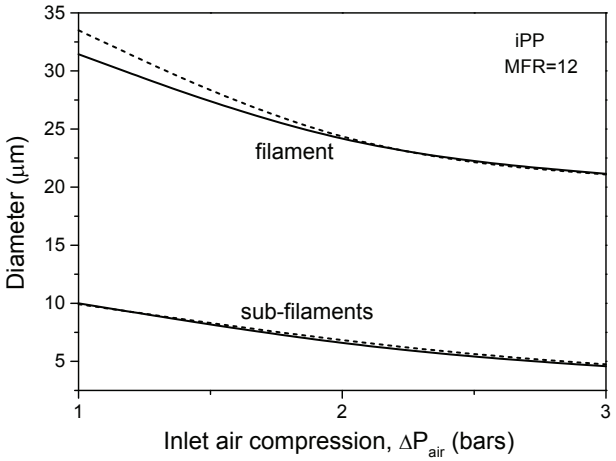

Fig. 6. *Diameter of iPP sub-filaments and filament without splitting vs. ΔP_{air} computed for zero-length nozzle throat (solid lines) and 8 mm long throat (dashed lines).*

REFERENCES

Bansal, V., Shambaugh, R.L., 1988, On-Line Determination of Diameter and Temperature during Melt Blowing of Polypropylene, *Ind. Eng. Chem. Res.,* 37, 1799-1806 .

Gerking, L., 2002, Nanoval Process for Spunbonded Nonwovens, *Chem. Fibers Int.*, 52, 424-426.

Gerking, L., 2004, Nanoval Process – Unique Hydrodynamic Effect (Part 1), *Chem. Fibers Int.*, 54, 261-262 .

Gerking, L., 2004, Nanoval Process for Spunbonded Details, *Chem. Fibers Int.*, 55, 52-56 .

Gerking, L., 2006, Nanoval Process – Unique Hydrodynamic Effect (Part 2), *Chem. Fibers Int.*, 56, 57-59.

Jarecki, L., Ziabicki, A., 2008, Mathematical Modeling of the Pneumatic Melt Spinning of Isotactic Polypropylene, Part II. Dynamic Model of Melt Blowing. *Fibres Text. Eastern Eur.,* 16, 17- 24.

Jarecki, L., Ziabicki, A., Lewandowski, Z., Blim, A., 2011, Dynamics of Air Drawing in the Melt Blowing of Nonwovens from Isotactic Polypropylene by Computer Modeling, *J. Appl. Polymer Sci*., 119, 53-65.

Krutka, H.M., Shambaugh R.L., Papavassiliou, D.V., 2003, Effects of Die Geometry on the Flow Field of the Melt Blowing Process, *Ind. Eng. Chem. Res.,* 42, 5541-5553 .

Lee, J.S., Shin, D.M., Jung, H.W., Hyun, J.C., 2005, Transient Solutions of the Dynamics in Low-Speed Fiber Spinning Process Accompanied by Flow-Induced Crystallization, *J. Non-Newtonian Fluid Mech*., 130, 110-116 .

Majumdar , B., Shambaugh, R.L., 1990, Air Drag on Filaments in the Melt Blowing Process *J. Rheol.,* 34, 591-601.

Larson, R.G., 1988, *Constitutive Equations for Polymer Melts and Solutions*, Butterworth, Boston.

Pope, S.B., 2000, *Turbulent Flows*, Cambridge University Press, Cambridge.

Roache, P.J., 1998, *Verification and Validation in Computational Science and Engineering*, Hermosa Publishers, Albuquerque, NM.

Wilcox, D.C, 1988, Reassessment of the Scale-Determining Equation for Advanced Turbulence Models, *AIAA Journal*, 26, 1299-1310.

Wilcox, D.C, 1988, Multiscale Models for Turbulent Flow, *AIAA Journal*, 26, 1311-1320.

Ziabicki, A., Jarecki L., Wasiak, A., 1998, Dynamic Modelling of Melt Spinning, *Comput. Theoret. Polimer Sci.,* 8, 143-157.

KOMPUTEROWE MODELOWANIE PROCESU PNEUMATYCZNEGO FORMOWANIA SUPERCIENKICH WŁÓKIEN

Streszczenie

Prezentowana jest komputerowa symulacja dynamiki nowego pneumatycznego procesu formowania supercienkich włókien ze stopu polimeru w naddźwiękowycm strumieniu powietrza z zastosowanie dyszy Lavala. Podejście bazuje na matematycznym modelu przepływu powietrza w dyszy Lavala oraz pneumatycznego rozciągania cienkich strug polimeru we współosiowym strumieniu powietrza. W pneumatycznym przędzeniu pola aerodynamiczne można rozważać jako niezaburzone obecnością pojedynczego szeregu cienkich strug polimeru i w modelowaniu procesu stosowane są pola predeterminowane wyznaczone na gruncie aerodynamicznego modelu *k-ω.* Pola aerodynamiczne są wyznaczone w przypadku kilku wartości ciśnienia powietrza na wejściu dyszy oraz dwu geometrii dyszy. Siła napędowa procesu z dyszą Lavala wynika z sił tarcia aerodynamicznego na powierzchni włókien. Zastosowano matematyczny model stacjonarnego przędzenia ze stopu polimeru w przybliżeniu pojedynczego, cienkiego włókna, z uwzględnieniem efektów nieliniowej lepkosprężystości stopu. Model pozwala również dyskutować nieliniowe właściwości elastooptyki wynikające z kształtującej się orientacji molekularnej, a także krystalizację polimeru w przypadku jej zachodzenia podczas formowania.

Przewidziano występowanie ujemnego ekstra-naprężenia reologicznego w pneumatycznie rozciąganym włóknie, wynikającego z nieliniowych właściwości lepkosprężystych stopu poddanego szybkiemu rozciąganiu. Ujemne ekstra-naprężenie może prowadzić do kawitacji w objętości włókna i podłużnego rozpryskowego rozszczepienia się włókna na dużą liczbę superienkich włókienek. Oszacowano z kryterium energetycznego hipotetyczną średnią wartość średnicy włókienek powstałych w wyniku rozszczepienia. Przykładowe obliczenia profili dynamicznych oraz dyskusja dotyczy procesu przędzenia w dyszy Lavala ze stopu izotaktycznego polipropylenu (iPP).

Received: October 13, 2010
Received in a revised form: October 20, 2010
Accepted: October 20, 2010